Mem. S.A.It. Vol. 86, 23

Memorie della

Spectral studies of FSRQs: constraining absorption models in the BLR at GeV energies

R. J. Britto[1], S. Razzaque[1], and B. Lott[2] on behalf of the Fermi-LAT Collaboration

[1] Department of Physics, University of Johannesburg, APK Campus, Auckland Park 2006, South Africa, e-mail: rbritto@uj.ac.za
[2] Centre d'Études Nucléaires de Bordeaux-Gradignan, Université Bordeaux 1, IN2P3/CNRS, 33175 Gradignan, France

Abstract. Flat spectrum radio quasars (FSRQs) are very bright and very distant active galactic nuclei (AGNs) surrounded by radiation fields from gas clouds at about 10^{17} cm from the central supermassive black hole. Absorption of gamma-rays inside this broad-line region (BLR) radiation field can trace the location of the gamma-ray emission region with respect to the outer limit of the BLR. We have analysed 5.5 years of data (2008-2014) from the Large Area Telescope (LAT) of the Fermi gamma-ray space observatory and performed spectral analysis of some bright FSRQs in the 100 MeV-200 GeV energy range. We modeled the absorption scenario within the BLR through the $\gamma\gamma$ absorption of > GeV photons interacting with Lyα, OVI and Lyβ photons. We discuss a possible constraint of the location of the GeV emission within the BLR.

Key words. Gamma rays: general – Galaxies: active nuclei – Galaxies: jets – Quasars: emission lines

1. Introduction

Blazars, a class of AGN, are among the most luminous objects of the Universe, and release a tremendous amount of energy through a pair of jets of plasma ejected at relativistic velocities. Blazar jets produce radiation across the whole electromagnetic spectrum, from radio waves to gamma-rays. They exhibit a characteristic double-bump spectral energy distribution (SED). The dominant radiation production process is understood to be synchrotron emission for the visible-UV range (first bump), whereas the X-ray/gamma-ray band (second bump) can be modeled by both leptonic and hadronic processes, although the inverse Compton process is most often used in modeling.

Flat spectrum radio quasars (FSRQs), a sub-class of blazars, are generally more luminous and at higher redshifts than the BL Lacs that constitute the other subclass of blazars. A specific characteristic of FSRQs is a broad-line emission spectrum that suggests the presence of clouds and intense radiation fields at a relatively close distance from the supermassive black hole. Gamma rays can be produced within the jet and/or by the interaction of the particles from the jets with visible and UV photons emitted in the broad-line region (BLR). If gamma-rays are produced within the BLR, it is expected that they would also undergo $\gamma\gamma \rightarrow e^{-}e^{+}$ interactions with BLR photons (Poutanen

& Stern 2010; Stern & Poutanen 2014). The radiation spectrum of the BLR would suggest that this absorption effect could be measured in the 10-100 GeV band. The Large Area Telescope (LAT) on-board the Fermi Gamma-ray Space Observatory is sensitive to gamma-rays between 20 MeV and 300 GeV (Atwood et al. 2009), and is the appropriate instrument for studying this effect and constraining the gamma-ray emission region within the BLR by fitting Fermi-LAT spectral data. Traditionally, the BLR was modeled as a spherical thick shell-type structure while more modern models assume a flat BLR (Tavecchio & Ghisellini 2012; Lei & Wang 2013).

We present our 5.5 yr Fermi-LAT data sample and the analysis procedure we used in Section 2. In Section 3 we present our modeling of the opacity $\tau_{\gamma\gamma}(E, z)$. We present our results and discuss perspectives on further studies in Section 4.

2. Data sample and analysis

We selected a sample of 8 bright FSRQs: PKS 1510-089 (redshift z=0.360), 4C +21.35 (also known as PKS 1222+216, z=0.434), 3C 279 (z=0.536), 3C 454.3 (z=0.859), 4C +55.17 (z=0.899), PKS 0454-234 (z=1.003), TXS 1520+319 (z=1.484), TXS 1520+319 (z=1.484) and PKS 1502+106 (z=1.839). We derived the BLR luminosity for each source, using (Pacciani et al. 2014; Xiong and Zhang 2014). We displayed these values in units of 10^{44} erg s^{-1}, in the order of the source list: 5.62, 15.80, 3.10, 33.00, 3.80, 3.70, 8.00 and 17.50. For each source, we analysed about 5.5 years of data (from August 2008 up to at least January 2014). The brightest flare ever detected in gamma-rays was seen from 3C 454.3 in Sep-Dec 2010 (Abdo at al. 2011). As such a flaring activity affects the shape of the 5.5 year SEDs, we present the results on this source without this high state period.

Our data analysis was performed using the public release of the Fermi Science Tools *v9r32p5-fssc-20130916*[1] and the instrument response function *PASS7_V15_SOURCE*. For each data sample, we considered all the photons from a region of 10 degree radius around the source of interest, and we estimated the signal contribution from other sources in a 20 degrees field-of-view, using an unbinned likelihood algorithm (*gtlike* science tool).

[1] http://fermi.gsfc.nasa.gov/ssc/data/analysis/

3. Modeling of the opacity of the BLR

We assume a model for the BLR luminosity and radius as $L_{BLR} = 0.1 L_{Disc}$ and $R_{BLR} = 10^{17}(L_{disc}/10^{45}\,\mathrm{erg\,s^{-1}})^{0.5}$ cm, respectively, where L_{Disc} is the accretion disc luminosity (Baldwin & Netzer 1978; Ghisellini & Tavecchio 2009). We also assume that BLR luminosity is dominated by Lyα and O VI+Lyβ lines with relative flux ratio 1 : 0.18 (Telfer et al. 2002). We model the Lyα and O VI+Lyβ lines as *Breit-Wigner* functions with peak energies $\epsilon_1 = 10.2$ eV and $\epsilon_2 = 12.04$ eV, with widths $\omega_1 = 0.8$ eV and $\omega_2 = 0.2$ eV, respectively. The $\gamma\gamma \to e^- e^+$ process has a threshold $E \approx 25.6/(1+z)$ GeV for Lyα photons, where E is the gamma-ray energy.

The differential opacity per unit distance for gamma-rays passing through the BLR will then be written as:

$$\frac{d\tau_{\gamma\gamma}}{dx}(E,z) = \frac{r_0^2}{2}\left[\frac{m^2c^4}{E(1+z)}\right]^2$$

$$\times \sum_{i=1}^{2}\left(n_i\omega_i \int_{\frac{m^2c^4}{E(1+z)}}^{\infty} \frac{\bar{\varphi}\left[\frac{\epsilon E(1+z)}{m^2c^4}\right] d\epsilon}{[(\epsilon-\epsilon_i)^2 + (\omega_i/2)^2]\epsilon^2}\right)$$

where $\bar{\varphi}$ is defined in Gould & Schréder (1967); Brown, Mikaelian & Gould (1973). Here

$$n_i \simeq 1.66 \times 10^{-11}\left(\frac{L_{i,45}}{\epsilon_{i,eV} R^2_{BLR,17}}\right)\,\mathrm{cm}^{-3},$$

with $L_1 = L_{BLR}/(1+f)$ for Lyα photons and $L_2 = f\,L_{BLR}/(1+f)$ for O VI+Lyβ photons, where $f = 0.18$.

The integrated opacity we obtain is $\tau_{\gamma\gamma}(E,z) = R_{BLR} \times \frac{d\tau_{\gamma\gamma}}{dx}(E,z)$.

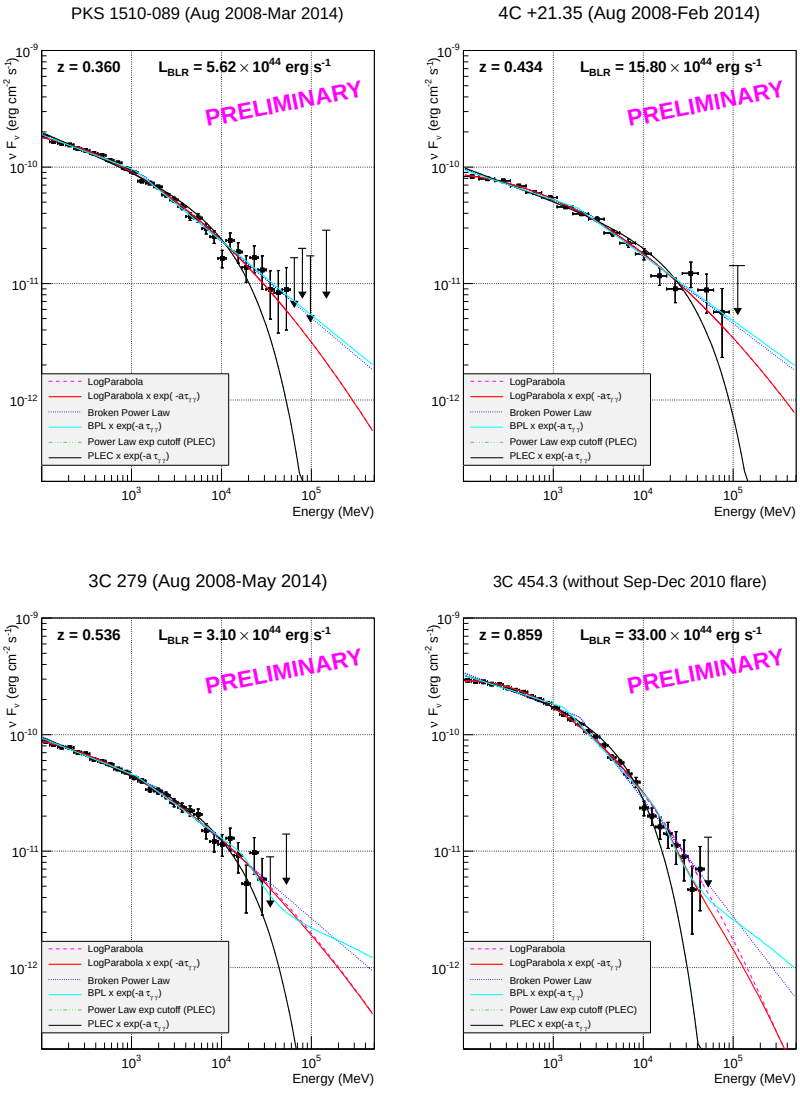

Fig. 1. SEDs of PKS 1510-089, PKS 1222+216 (4C +21.35), 3C 279 and 3C 454.3. *PLEC* and *LP* fits are often hidden beneath *PLEC*τ and *BPL*τ.

4. Preliminary results and discussion

We produced the SEDs of the 8 bright sources we presented earlier between 100 MeV up to a few tens of GeV. Fig. 1 presents the three TeV sources—PKS 1510-089, 4C +21.35 (also called PKS 1222+216), and 3C 279—and 3C 454.3. In Fig. 2 higher redshift sources ($z \geq 0.9$) are presented: 4C +55.17, PKS 0454-234, TXS 1520+319 and PKS 1502+106. The LAT data points are not corrected for the absorption of extragalactic background radiation (*i.e.* not de-absorbed), which is expected to be a small correction below 100 GeV.

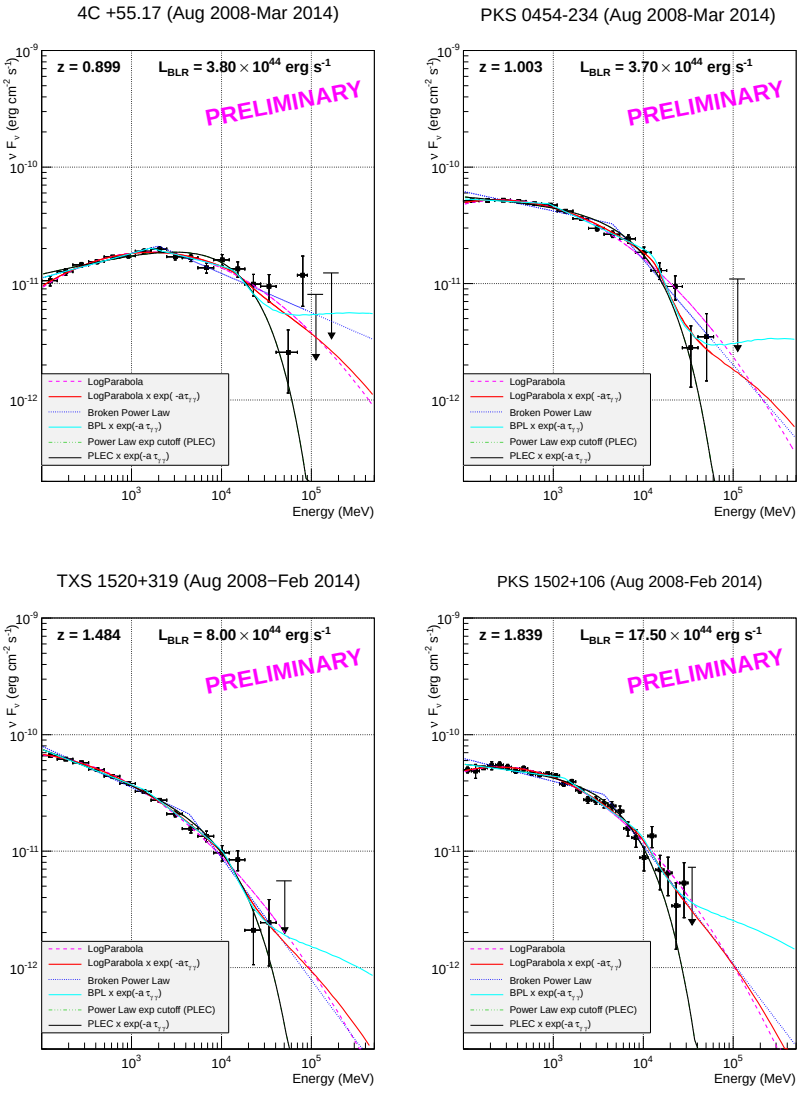

Fig. 2. SEDs of 4C +55.17, PKS 0454-234, TXS 1520+319 and PKS 1502+106. *PLEC* and *LP* fits might be hidden beneath $PLEC\tau$ and $BPL\tau$.

Most of the FSRQ SEDs are usually well fitted using at least one of the three following functions in the MeV-GeV range: a *log-parabola (LP)*, defined in this paper as $N(E) = N_0\ (E/1000\ MeV)^{-\alpha-\beta\ log(E/1000\ MeV))}$; a *broken power law (BPL)*, defined as $N(E) = N_0\ (E/E_b)^{-\Gamma_i}$, with $i = 1$ if $E < E_b$ and $i = 2$ if $E > E_b$; a *power law with an exponential cutoff (PLEC)*, defined as $N(E) = N_0\ (E/1000\ MeV)^{-\Gamma}\ \exp(-E/E_c)$. We use

Table 1. Fitting parameters and derived significances, for the three TeV sources and 3C 454.3 without the Sep-Dec 2014 high state. We indicate with (*) when a reached the lower edge of the interval for fitting.

Param	Model		PKS 1510-089 (z=0.360)	4C +21.35 (z=0.434)	3C 279 (z=0.536)	3C 454.3 (no flare) (z=0.859)
function *(without absorption model)*	LP	α	2.442 ± 0.010	2.337 ± 0.014	2.424 ± 0.013	2.485 ± 0.009
	LP	β	0.063 ± 0.006	0.056 ± 0.010	0.055 ± 0.008	0.111 ± 0.005
	BPL	Γ_1	2.321 ± 0.015	2.278 ± 0.026	2.341 ± 0.016	2.295 ± 0.012
	BPL	Γ_2	2.655 ± 0.041	2.587 ± 0.080	2.662 ± 0.076	3.004 ± 0.037
	BPL	E_{break}	1392 ± 226.9	2465 ± 896.0	2088 ± 506.9	1972 ± 0.1
	PLEC	Γ	2.325 ± 0.019	2.283 ± 0.032	2.311 ± 0.020	2.217 ± 0.018
	PLEC	E_{cutoff}	16023 ± 2966.8	33678 ± 11941	16369 ± 3490.4	6770 ± 657.4
function *(with absorption model)*	LPτ	α	2.442 ± 0.010	2.337 ± 0.014	2.423 ± 0.014	2.478 ± 0.011
	LPτ	β	0.063 ± 0.006	0.056 ± 0.010	0.054 ± 0.009	0.108 ± 0.006
	BPLτ	Γ_1	2.295 ± 0.016	2.257 ± 0.028	2.309 ± 0.020	2.247 ± 0.012
	BPLτ	Γ_2	2.630 ± 0.042	2.560 ± 0.065	2.561 ± 0.053	2.835 ± 0.031
	BPLτ	E_{break}	1092 ± 180.0	1862 ± 614.8	1128 ± 274.6	1308 ± 0.1
	PLECτ	Γ	2.325 ± 0.019	2.284 ± 0.032	2.311 ± 0.020	2.217 ± 0.019
	PLECτ	E_{cutoff}	16022 ± 2967.3	33695 ± 11961	16370 ± 3491.6	6769 ± 657.6
a	LP		0.00001*	0.00001*	0.0014 ± 0.066	0.003 ± 0.003
	BPL		0.0003 ± 0.037	0.00001*	0.0143 ± 0.020	0.006 ± 0.003
	PLEC		0.00001*	0.00001*	0.00001*	0.00001*
χ^2 (ndf) *(without abs. model)*	LP		14.700 (28)	4.894 (14)	7.306 (25)	12.925 (27)
	BPL		23.265 (27)	8.759 (13)	15.286 (24)	50.945 (26)
	PLEC		42.140 (28)	15.093 (14)	13.670 (25)	46.111 (27)
χ^2 (ndf) *(with abs. model)*	LPτ		14.702 (27)	4.898 (13)	7.301 (24)	11.577 (26)
	BPLτ		16.377 (26)	8.025 (12)	11.127 (23)	33.952 (25)
	PLECτ		42.144 (27)	15.098 (13)	13.671 (24)	46.120 (26)
p-value	LP		9.588e-01	9.487e-01	9.427e-01	2.455e-01
	BPL		8.680e-03	3.917e-01	4.141e-02	-
	PLEC		-	9.475e-01	9.748e-01	9.227e-01

these functions to fit the SEDs presented in this paper from 100 MeV up to the last data point preceding an upper limit.

We also performed another set of three fits, by a convolution of each of the previous functions with $\exp(-a\ \tau_{\gamma\gamma}(E,z))$, where a is an additional parameter that represents the fraction of the BLR in which the gamma-ray photons are traveling/absorbed, assuming the hypothesis of the previous section. In this case, the observed flux would be $F_{obs}(E) = e^{-\tau_{\gamma\gamma}(E,z)}F_{int}(E)$, and these new fit functions will be referred to hereafter as $LP\tau$, $BPL\tau$ and $PLEC\tau$.

We show the fit parameters of all six fits of each SED in Table 1 and 2, corresponding to the plots of Figure 1 and 2. When we consider the fits performed with the LP, BPL and PLEC functions, we note that the χ^2/ndf of LP is good for all the sources ($\sim$ 1). It gives better fits than BPL and PLEC, except in the case of PKS 1510-089 and TXS 1520+319 (χ^2/ndf of BPL and PLEC respectively are similar to their LP one). Now we use the $LP\tau$, $BPL\tau$ and $PLEC\tau$ set of fits that carries information about the opacity $\tau_{\gamma\gamma}$. The best fit is obtained by optimising a within a search interval between 0.00001 and 1 in our fitting programs, as a representation of the fraction of the BLR in which the gamma-ray absorption may occur. In many cases, a takes the value 0.00001 ('at limit'), and in those case the corresponding fit is matching the fit without the $\exp(-a\ \tau_{\gamma\gamma})$ factor (fitting line superimposed on the figure and hiding the previous line). We acknowledge that the a's have large errors, due to large error bars in the $\gtrsim 10\ GeV$ regime were the contribution of $\tau_{\gamma\gamma}(E,z)$ becomes significant. Note that fitting the data points with the $\exp(-a\ \tau_{\gamma\gamma})$ factor leads to improvements in the χ^2/ndf values in many cases. While comparing each *absorption model fit* with its corresponding fit (LP, BPL or PLEC), and if both fits have a $\chi^2/ndf \leq 1$, we obtain a $p-value$ which indicates the discrepancy between the fit with model and the fit without model, for a given function. However $p-value$ is always above 3×10^{-3} (less than 3 σ), except for PKS 1510-089, but a is compatible with 0 for this source. Only the higher redshift sources PKS 0454-234 and PKS 1502+106 have a parameter a with an error bar less than half the parameter

Table 2. Fitting parameters and derived significances for the four high redshift sources. We indicate with (*) when a reached the lower edge of the interval for fitting.

Param	Model		4C +55.17 (z=0.899)	PKS 0454-234 (z=1.003)	TXS 1520+319 (z=1.484)	PKS 1502+106 (z=1.839)
function *(without absorption model)*	LP	α	1.914 ± 0.021	2.233 ± 0.015	2.436 ± 0.019	2.300 ± 0.014
	LP	β	0.093 ± 0.011	0.089 ± 0.009	0.079 ± 0.011	0.110 ± 0.009
	BPL	Γ_1	1.788 ± 0.036	2.168 ± 0.018	2.355 ± 0.028	2.197 ± 0.014
	BPL	Γ_2	2.336 ± 0.052	2.903 ± 0.099	3.050 ± 0.258	3.011 ± 0.152
	BPL	E_{break}	1996 ± 315.4	4569 ± 5	4395 ± 1613.3	3664 ± 572
	PLEC	Γ	1.820 ± 0.025	2.063 ± 0.025	2.287 ± 0.037	2.066 ± 0.023
	PLEC	E_{cutoff}	16605 ± 2984.7	11658 ± 2141.7	13679 ± 3537.6	7349 ± 913.0
function *(with absorption model)*	LPτ	α	1.914 ± 0.020	2.212 ± 2.212	2.417 ± 0.026	2.288 ± 0.017
	LPτ	β	0.085 ± 0.015	0.072 ± 0.072	0.067 ± 0.017	0.101 ± 0.012
	BPLτ	Γ_1	1.788 ± 0.036	2.042 ± 2.042	2.304 ± 0.033	2.104 ± 0.018
	BPLτ	Γ_2	2.192 ± 0.065	2.363 ± 2.363	2.594 ± 0.136	2.547 ± 0.074
	BPLτ	E_{break}	1626 ± 320.6	880 ± 880	1423 ± 752.9	1317 ± 206
	PLECτ	Γ	1.820 ± 0.025	2.064 ± 2.064	2.287 ± 0.037	2.066 ± 0.023
	PLECτ	E_{cutoff}	16607 ± 3068.5	11660 ± 11660	13683 ± 3538.1	7350 ± 914
a	LP		0.005 ± 0.007	0.020 ± 0.009	0.008 ± 0.007	0.004 ± 0.003
	BPL		0.015 ± 0.006	0.031 ± 0.009	0.013 ± 0.008	0.007 ± 0.003
	PLEC		0.00001*	0.00001*	0.00001*	0.00001*
χ^2 (ndf) *(without abs. model)*	LP		12.768 (14)	7.993 (13)	5.546 (12)	16.056 (25)
	BPL		18.258 (13)	35.170 (12)	10.548 (11)	69.639 (24)
	PLEC		25.300 (14)	16.315 (13)	5.392 (12)	32.431 (25)
χ^2 (ndf) *(with abs. model*	LPτ		12.201 (13)	3.451 (12)	4.404 (11)	14.622 (24)
	BPLτ		11.948 (12)	3.777 (11)	6.391 (10)	26.473 (23)
	PLECτ		25.304 (13)	16.317 (12)	5.395 (11)	32.440 (24)
p-value	LP		4.514e-01	3.307e-02	2.852e-01	2.311e-01
	BPL		1.201e-02	-	4.148e-02	-
	PLEC		-	9.643e-01	9.636e-01	9.234e-01

value for $BPL\tau$ and a relatively small χ^2/ndf. Though we cannot compare these $BPL\tau$ fits with their corresponding BPL fits that have a bad χ^2/ndf, we can still consider this result as showing a potential absorption that should be confirmed by more statistics. PKS 0454-234 has also a good χ^2/ndf for the $BPL\tau$ fits, with $a = 0.031 \pm 0.009$. However, as χ^2/ndf of BPL is not good enough, we cannot discuss the significance of the fit discrepancy. Since we do not see evidence of a strong gamma-ray absorption, this indicates that the production of gamma-rays should not happen deep within the BLR, where the optical/UV photon flux density is higher. We are planning to study more sources and to produce sub-datasets in given time intervals corresponding to flaring activities to continue this study. 3C 454.3 is a good candidate to pursue quiescent *versus* flaring state comparison.

Acknowledgements. The *Fermi*-LAT Collaboration acknowledges support for LAT development, operation and data analysis from NASA and DOE (United States), CEA/Irfu and IN2P3/CNRS (France), ASI and INFN (Italy), MEXT, KEK, and JAXA (Japan), and the K.A. Wallenberg Foundation, the Swedish Research Council and the National Space Board (Sweden). Science analysis support in the operations phase from INAF (Italy) and CNES (France) is also gratefully acknowledged.

References

Abdo, A. A., et al 2011, ApJ, 733, L26
Atwood, W. B., et al 2009, ApJ, 697, 1071
Baldwin, J. A., and Netzer, H. 1978, ApJ, 226, 1
Brown, R. W., Mikaelian, K. O., and Gould, R. J. 1973, ApJ, 14, L203
Ghisellini, G. and Tavecchio, F. 2009, MNRAS, 397, 985
Gould, R. J. and Schréder, G. P. 1967, Physical Review, 155, 5
Lei, M. and Wang, J. 2014, PASJ, 66, 1,
Pacciani, L., et al 2014, arXiv:1312.3998v2
Poutanen, J. and Stern, B. 2010, ApJ, 717, L118
Stern, B. and Poutanen, J. 2014, ApJ, in press, arXiv:1408.0793v1
Telfer, R. C., Zheng, W., Kriss, G. A., and Davidsen, A. F. 2002, ApJ, 565, 773
Tavecchio, F., & Ghisellini, G. 2012, arXiv:1209.2291

Xiong, D. R. and Zhang, X. 2014, MNRAS, 441, 3375